Desalination 496 (2020) 114647

Contents lists available at ScienceDirect

Desalination

journal homepage: www.elsevier.com/locate/desal

Water desalination with nickel hexacyanoferrate electrodes in capacitive deionization: Experiment, model and comparison with carbon

K. Singh[a,b], L. Zhang[b], H. Zuilhof[a,c,d], L.C.P.M. de Smet[a,b,*]

[a] Laboratory of Organic Chemistry, Wageningen University, the Netherlands
[b] Wetsus, European Centre of Excellence for Sustainable Water Technology, Leeuwarden, the Netherlands
[c] School of Pharmaceutical Sciences and Technology, Tianjin University, Tianjin, China
[d] Department of Chemical and Materials Engineering, Faculty of Engineering, King Abdulaziz University, Jeddah, Saudi Arabia

ARTICLE INFO

Keywords:
Capacitive deionization
Prussian blue analogues
Water desalination

ABSTRACT

Capacitive deionization (CDI) is a water desalination technology in which ions are removed from water by creating a potential difference between two capacitive electrodes. Porous carbon has been extensively used as an electrode material in CDI. However, recent developments in the field of intercalation materials have led to their application in CDI due to their large ion storage capacity. One such intercalation material, nickel hexacyanoferrate (NiHCF), was used in this study as the electrode material. A symmetrical cell was assembled with two identical NiHCF electrodes separated by an anion-exchange membrane. The effect of operational parameters such as current density, feed concentration and flow rate on the desalination characteristics of the cell was investigated. The highest salt adsorption capacity of ≈ 35 mg/g was measured at a current density of 2.5 A/m^2 in a 20 mM NaCl feed solution. Furthermore, a Nernst-Planck transport model was successfully used to predict the change in the outlet concentration and cell voltage of the symmetric CDI cell. Finally, performance of the symmetric NiHCF CDI cell was compared with an MCDI cell with porous carbon electrodes. The NiHCF cell, on average, consumed 2.5 times less energy than the carbon-based MCDI cell to achieve similar levels of salt removal from saline water in CDI.

1. Introduction

Capacitive deionization (CDI) is an electrochemical water desalination technique in which the anions and cations are removed from water and temporarily stored in capacitive electrodes by creating a potential difference between them [1–3]. Regardless of the similarities between the design of different desalination setups, the mechanism of ion storage in the capacitive electrodes marks the difference between CDI and other electrochemical technologies such as electrodialysis, ED, where desalination is driven by faradaic reactions occurring at the electrodes. Therefore, desalination *via* ED can function continuously, provided the reaction conditions are maintained. On the other hand, conventional CDI cells produce desalinated water in an intermittent manner and the electrode voltage changes with charge accumulation. Once saturated, the capacitive electrodes are regenerated by either short-circuiting or reversing the polarities. This regeneration step interrupts the desalinated water supply. However, a different cell architecture such as flow electrodes and rocking chair can enable CDI to continuously produce desalinated water [4–6], similar to ED and reverse osmosis. Moreover, it has been demonstrated that a part of the electrical energy supplied to the electrodes during the ion adsorption step can be recovered, after adjusting for the resistive losses, during the desorption step [7,8]. The recovery of the energy released during the electrode regeneration can enhance the thermodynamic energy efficiency of CDI [9], making capacitive electrodes attractive for water desalination applications.

Conventionally, porous carbon has been used as an electrode material in CDI [10–13], due to its low cost, high specific surface area and electronic conductivity. Ion storage in these electrodes proceeds *via* an electrical double layer (EDL) formation on the pore surface [14]. However, carbon electrodes in CDI suffer from co-ion expulsion *i.e.* the depletion of co-ions from the EDL during counter-ion adsorption [15]. This results in only a partial use of the applied current or the potential difference in storing counter-ions in the micropores of the carbon electrodes, as the remaining part is diverted towards the removal of co-ions from the micropores. As a consequence, the energy and thermodynamic efficiency of the process decreases. It can be solved by placing ion-exchange membranes, IEMs, in between the electrodes and the flow

* Corresponding author at: Laboratory of Organic Chemistry, Wageningen University, the Netherlands.
E-mail address: louis.desmet@wur.nl (L.C.P.M. de Smet).

https://doi.org/10.1016/j.desal.2020.114647
Received 28 May 2020; Received in revised form 15 July 2020; Accepted 20 July 2020

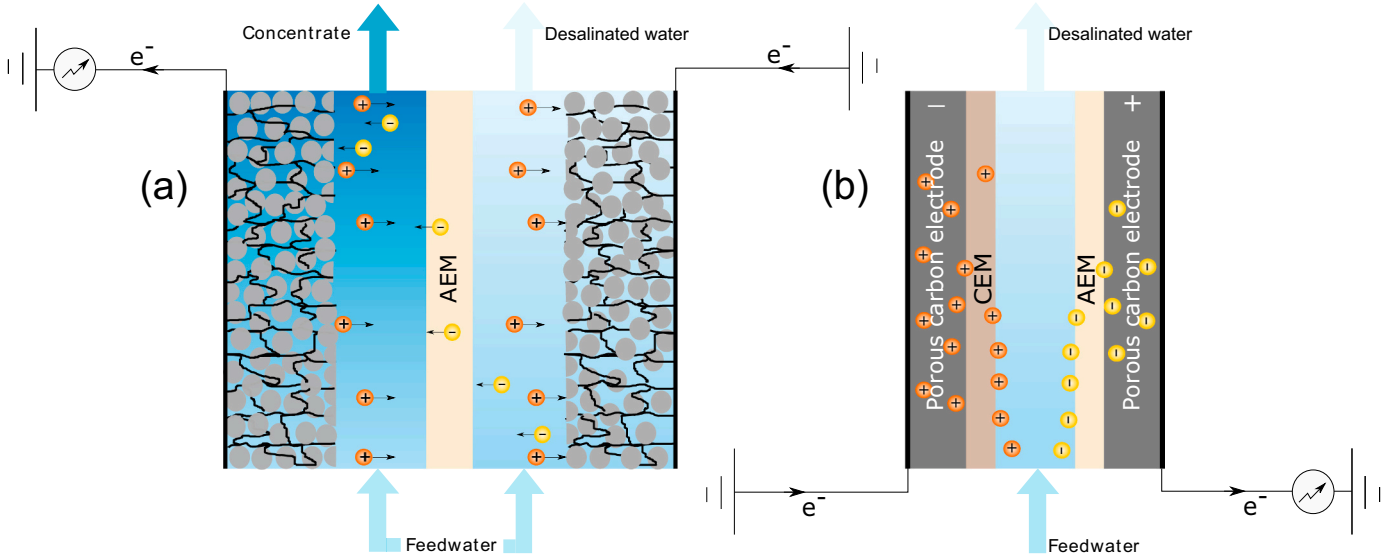

Fig. 1. Schematics of the two CDI setups, one with PBA and the other with porous carbon electrodes **(a)** A two-compartment symmetric cell assembled with identical NiHCF electrodes separated by a pair of flow channels and an AEM. The active particles, grey spheres, are presented as an agglomerate connected to each other and to the current collector, black solid line adjacent to the electrodes, by the conductive carbon, represented by twisted black lines running across the width of the electrode. **(b)** A one-compartment MCDI cell with identical porous carbon electrodes. In this configuration, an AEM and CEM are placed in front of the carbon electrodes, separating them from the flow channel in the middle.

channel, effectively blocking the release of the co-ions from the micropores [16]. This is called membrane capacitive deionization, MCDI. Furthermore, the ion storage in the electrical double layers shows limited inherent selectivity towards different ions [17–19], restricting its use in selective ion-exchange membranes.

Recently, intercalation materials, explored in the field of batteries, have found application in electrode materials as an alternative to the porous carbon in CDI [20,21]. The ion storage in these materials involves insertion of an ion, mostly cation, in interstitial sites [22]. This mechanism is advantageous, as it has the desirable characteristics of adsorption in carbon such as fast kinetics [23] and improves upon the ion storage capacity [24], while eliminating the co-ion repulsion. In addition, desalination systems based on intercalation materials provide more flexibility for selective removal of ions of choice [25–28] without any chemical modifications of the electrode. Finally, the intercalation electrodes are capable of storing the same amount of charge at a lower voltage, which can lower their energy consumption in comparison to their carbon-based counterparts, as argued in [6] and recently predicted theoretically in [29]. Here, we focus on this energy aspect of the intercalation materials and compare them with carbon electrodes.

Among all the intercalation materials, the so-called Prussian blue analogues (PBAs) have been most commonly used to fabricate electrodes for CDI cells [6,30–32]. These materials have attracted attention due to their non-toxic nature, open framework structure, customizable chemistry, and stability at high cycling rates [33]. The process of intercalation in these materials proceeds *via* the insertion of a cation in an interstitial lattice site and a simultaneous reduction of a redox-active species in the cubic lattice structure [33]. The deintercalation of the inserted ion, during regeneration, is accompanied by the oxidation of the same redox-active species, thus maintaining the electro-neutrality of the lattice. An ideal PBA unit cell has an empirical formula of $A_2M[Fe(CN)_6]$ where A is an alkali metal (Na, K) and M can be Ni [34], Cu [35], V [23] or other transition metal elements [33,36]. This highlights the versatility of the chemical composition of PBAs. In addition, PBAs have demonstrated an ability to intercalate ions of multiple valences such as Na^+, Ca^{2+}, and Y^{3+} among others [34,37]. One such PBA, NiHCF, with $Na_2Ni[Fe[(CN_6)]$ as empirical formula of its reduced form, is used in this study as an electrode material for water desalination. The lattice structure in this material is important since a highly crystalline structure would result in a higher charge storage capacity, which is inversely proportional to the defects in the crystal structure such as the absence of $Fe(CN)_6$ from the lattice. The loss of storage capacity in NiHCF electrodes has been attributed to the irreversible oxidation of the redox-active materials instead of the process of (de)intercalation [38].

The use of intercalation materials such as NiHCF as an alternative to porous carbon in CDI relies upon **(a)** desalination performance metrics such as energy consumption and productivity, P, defined as the volume of desalinated stream produced over a cycle for a given electrode area and **(b)** desalination objectives such as an average reduction in concentration with respect to inlet feed, c_{in}, $\langle \Delta c \rangle$, and water recovery (WR) for a given inlet feed concentration. The desalination performance indicators such as the salt adsorption capacity, SAC, and the charge efficiency in combination with the metrics can further help in assessment of electrode material performance in CDI. Many studies have reported a higher SAC for intercalation electrodes in comparison to that of carbon [6,31,39,40]. However until now, there has been no effort to compare the performance of intercalation electrodes with that of carbon electrodes, in terms of well-defined performance metrics, under equivalent separation conditions and cell design elements [20,41]. The current study bridges this gap by providing a direct comparison between an intercalation electrode based-symmetric cell and a porous carbon electrode-based MCDI cell with respect to specific performance metrics, indicators, and separation conditions as described elsewhere [41]. The cell used in this study is termed symmetric as the electrodes in the cell intercalate the same kind of ion *i.e.* cation [4]. A comparison, as presented in this work, will help to put the performance of intercalation electrodes in perspective with that of porous carbon electrodes. In addition, it will facilitate the comparison of CDI systems based on symmetric intercalation electrodes with other desalination technologies as the comparisons currently presented in literature, with reverse osmosis and electrodialysis, take neither the intercalation materials nor the symmetric cell configuration in CDI into account [42,43].

In this study, we use two NiHCF electrodes, with identical chemical and ionic composition, in a symmetrical CDI cell configuration to desalinate feed water containing NaCl. The electrodes are referred to as identical here if their ionic content is the same. An estimate of their state of charge/discharge is defined as the intercalation degree, ϑ, which ranges between 0 and 1, and is calculated by taking a ratio of the

actual charge transferred to or from the electrode and the equilibrium charge storage capacity of the electrode. A $\vartheta \approx 0$ indicates a state of minimum Na^+ content (charge) and $\vartheta \approx 1$ indicates the maximum Na^+ content (discharge) inside the NiHCF particles. A schematic in Fig. 1 (a) shows the symmetric cell with NiHCF electrodes under operation in a desalination cell. The figure shows the moment during which a current applied *via* the external circuit results in a synchronized expulsion and introduction of electrons from the left and the right electrode, respectively. In this moment, Na^+ deintercalates from the left electrode into the solution. It is mirrored in the right compartment where Na^+ intercalates into the electrode. Both of these processes occur simultaneously to preserve the electroneutrality. The electric field drives the Cl^- in the direction opposite to that of Na^+ from the spacer channel. Therefore, an anionic flux is directed through the anion-exchange membrane (AEM) towards the electrode on the left. The Na^+ deintercalating from the anode combines with the Cl^- migrating through the membrane to give a concentrated stream in the anodic compartment and a fresh water stream in the cathodic compartment. This study also includes the influence of c_{in} and applied current densities I on the $\langle \Delta c \rangle$, energy consumed per cubic meter of the desalinated water, and the SAC. In addition, a theoretical model for symmetric CDI cell with intercalation materials such as NiHCF, developed in [44], was used to describe the results obtained from experiments. The theoretical description, reported here with the experimental results, gives insight into desalination by the symmetric NiHCF cell. Finally, a comparison between symmetric CDI cell with NiHCF electrodes and an MCDI cell with porous carbon electrodes, as depicted in Fig. 1 (b), was performed. The MCDI cell resembled the symmetric cell with the PBA electrodes by having the same geometric surface area (cm^2) and loading (g-active material/cm^2), spacer porosity and thickness along with the graphite current collectors and the polymeric end-plates. In addition to an AEM, the MCDI cell had a cation-exchange membrane, CEM, for the cathode. The performance metrics and indicator mentioned in [41], such as the energy consumption, P, and $\langle \Delta c \rangle$, respectively, were evaluated under identical experimental conditions for the symmetric cell with NiHCF electrodes and for the MCDI cell with porous carbon electrodes to highlight the differences between them. A list of symbols used throughout the manuscript is provided in Table 1.

2. Materials and methods

2.1. NiHCF synthesis and characterization

A co-precipitation method [45] was adopted to prepare the NiHCF powder. A 200 mL solution of 24 mM $NiCl_2 \cdot 6H_2O$ (Alfa Aesar) and 12 mM $Na_4Fe[(CN)_6]\cdot 10H_2O$ (Sigma Aldrich) each was added dropwise to a 200 mL reaction medium containing 99% milliQ water and 1% 1 M HCl, by volume, under vigorous stirring. The reaction mixture was stirred at 1000 RPM for ≈ 12 h. The precipitate formed was washed three times with MilliQ water using a vacuum filtration unit and dried overnight in a vacuum oven at 40 °C. The chemical composition of the powder was determined by dissolving a small amount of NiHCF precipitate in a ≈ 70% (by volume) solution of HNO_3, and using inductive coupled plasma optical emission spectrometry (ICP-OES) to analyse the resulting solution. The surface morphology of the NiHCF was observed using a scanning electron microscope (SEM). The particles were coated with gold and imaged under the microscope for two different magnifications. The Brunauer-Emmett-Teller, BET, surface area of the NiHCF powder and the YP 80F carbon was measured by Tristar 3000 surface area analyser (Micromeritics). The crystallinity of the NiHCF particles was assessed by powder X-ray diffraction (XRD) analysis, performed using a copper source for diffraction angles in the range of $10^\circ < 2\theta < 80^\circ$.

Table 1
List of symbols.

Nomenclature			
Applied current density (A/m^2)	I	Intercalation degree	ϑ
Inlet concentration (mM)	c_{in}	Spacer/electrode porosity	ρ_s/ρ_e
Change in concentration (mM)	Δc	Spacer/electrode tortuosity	$\varepsilon_s/\varepsilon_e$
Average concentration change (mM)	$\langle \Delta c \rangle$	Dimensionless potential	ϕ
Maximum cation concentration (M)	c_{max}	Dimensionless potential in electrode	ϕ_{ec}
Reference concentration (mM)	c_{ref}	Inter-ionic repulsion factor	g
Concentration in active particle (mM)	c^+	Fluid velocity in flow direction (m/s)	v_y
Interfacial area (cm^2)	A	Ion valency i	z_i
Active particle volume fraction	ε_a	Intercalation flux (mol/m^3s)	aJ_{int}
Volumetric flow rate (mL/min)	Q	Productivity ($L/h/m^2$)	P
Half cycle time (s)	Δt_{HCT}		

2.2. Electrode preparation and characterization

The dried NiHCF precipitate, obtained from the co-precipitation reaction mentioned in Section 2.1, was used as an active material in preparing free-standing electrodes for desalination experiments. These electrodes comprised of conductive carbon black (Cabot), to enhance the electronic conductivity of the electrodes, and poly-tetrafluroethylene (PTFE) (Sigma Aldrich), to provide them shape and bind the components together. The NiHCF precipitate and the conductive carbon were milled together. The fine NiHCF-carbon blend was mixed with the 60% (by weight) PTFE dispersion and ethanol as a solvent. The slurry formed contained the NiHCF powder, carbon black and the binder in a ratio of 8:1:1 by weight. The slurry was kneaded until the majority of the solvent evaporated. The electrode mass left behind, in form of a wet dough, was cold rolled into 200 μm sheet electrodes with stainless steel rollers in a rolling machine (MTI corp.) at room temperature. Finally, the electrodes were cut into rectangles of 10 cm × 2 cm, dried in an oven at 60 °C for 2 h to eliminate any residual ethanol from the fabrication procedure and weighed. The weight of the electrodes was kept between 0.42 and 0.45 g.

Electrodes were electrochemically characterized by an *ex-situ* Galvanostatic Intermittant Titration Technique, GITT. A three-electrode cell setup was employed in this technique containing the NiHCF electrode as the the working electrode (WE), a platinum-coated titanium mesh as the counter electrode (CE) and a Ag/AgCl electrode as the reference electrode (RE). A 1 M Na_2SO_4 solution, bubbled with nitrogen, was used as an electrolyte. The pH of the electrolyte was monitored at specific intervals and kept acidic (pH = 3). Current was applied in pulses *via* a potentiostat (IviumStat.h standard, IVIUM Technologies), and the corresponding voltage response was recorded. These current pulses were interrupted by an equilibration time, during which the circuit was left open and the open circuit voltage (OCV) was measured. The number of pulses applied to the cell corresponds to the charge capacity of the WE. Each pulse carried a charge of 5C (at a current of ≈ 60 mA/g-NiHCF). The charge storage capacity of the electrodes was determined by the product of the number of (de)intercalation steps and the charge transferred to the electrodes in these steps.

The carbon electrodes used in the MCDI cell were prepared in a similar manner as the NiHCF electrodes. In place of NiHCF, fine YP 80F carbon powder was used. The ratio of YP 80F and PTFE in the resulting electrodes was 0.95:0.05. The thickness of carbon electrodes was kept at ≈ 700 μm to keep their area and weight equal to that of the 200 μm thick NiHCF electrodes. The electrochemical characterization of the YP 80F carbon electrodes has been reported in detail elsewhere [46].

2.3. Cell assembly and experiments

The NiHCF electrodes were pre-treated prior to the assembly of the desalination cell. One of the two NiHCF electrodes used in the

desalination cell, as shown in Fig. 1 (a), was put in a three-electrode cell configuration and charged to 0.9 V to deintercalate the cations, Na^+ in this study, from the interstitial sites in it. The other electrode was assembled in an identical cell and discharged to −0.2 V to intercalate cations in the interstitial sites of the active particles bringing the electrode to a state of maximum discharge. These charged and discharged electrodes were then assembled in the desalination cell of Fig. 1 (a) together with spacer channels, an AEM, graphite current collectors and PVC end plates to sandwich the arrangement together. After the assembly, the cell was short-circuited for 1 h. This step before starting the desalination experiment was performed to equalize the ion content in the two, fully intercalated and deintercalated, electrodes. This ensures that the desalination starts with two identical electrodes, resulting in symmetrical and mirrored operation in the two cell chambers.

The MCDI desalination cell with carbon electrodes was assembled according to the schematic presented in Fig. 1 (b). The cell design elements including the electrode weight of 0.45 g, projected area of 20 cm^2 and spacer thickness of 500 μm were kept identical to the symmetric CDI cell with NiHCF electrodes. The spacer channel was separated from the anode and cathode by the AEM and the CEM (CMX Neosepta), respectively. The carbon electrodes were soaked in the feed water for 0.5 h before the assembly.

Two sets of experiments were performed to investigate the performance of NiHCF electrodes and to allow comparison with literature. In the first set, constant current was applied to the symmetric cell with NiHCF electrodes in the cell voltage window of ± 1 V to desalinate feed with c_{in} of 5, 20, and 50 mM NaCl. For all these concentrations, I was varied from 2.5 to 15 A/m^2. The current was normalized with the projected electrode area of 20 cm^2. The change in effluent concentration was monitored using a probe, connected to a conductivity meter (Orion Versa star, Thermo Scientific), at the two outlets of the desalination cell. The SAC obtained during the a half cycle was determined as

$$\frac{QM}{m}\int_{\Delta t_{HCT}}\left(c_{in}-c_{out}\right)dt, \tag{1}$$

where c_{out} indicates effluent concentration, M is the molar mass of NaCl, Q is the feed flow rate through each spacer channel, Δt_{HCT} is the half cycle time for the adsorption/desorption steps and m is the weight of both electrodes in the desalination cell. The symmetric cell with the NiHCF electrodes removes salt from both compartments over the entire duration of the desalination cycle. Therefore, the total salt removed in one full cycle is different from the SAC and is obtained by the addition of the SAC obtained during the adsorption half cycles of each electrode.

In the second set of experiment, the half cycle time, Δt_{HCT}, of the adsorption and desorption steps was fixed. The NiHCF cell was operated under both constant current and constant voltage modes. The c_{in} of the feed was kept constant at 20 mM NaCl. During the operation, I was varied in the range of 10 to 30 A/m^2, and the Q was varied in the range of 4–12 mL/min. For operation in constant voltage mode, the cell voltage was varied from 0.4 to 1.2 V. For example, in one cycle, +0.4 V was applied in the first half and −0.4 V was applied in the second half of the cycle. This procedure was repeated for the cell voltages 0.6, 0.8, 1, and 1.2 V. For all these experiments, the c_{in} and Q was kept constant at 20 mM and 7.8 mL/min, respectively.

Finally, for direct performance comparison, the symmetric cell with NiHCF electrodes and the MCDI cell with carbon electrodes were operated under the identical constant current conditions for the same c_{in}, Δt_{HCT} and Q. The $\langle \Delta c \rangle$ was calculated as

$$\langle \Delta c \rangle = \frac{N_d}{V_d}, \tag{2}$$

where N_d are the moles of salt removed from the feed in one cycle and V_d is the volume of feed desalinated in one cycle. The average salt adsorption rate (ASAR) over a desalination cycle was calculated in two ways, as described in [41], in two units:

$$\mathrm{ASAR(mg/g/min)} = \frac{\mathrm{SAC}}{\Delta t_{cycle}}, \tag{3}$$

and

$$\mathrm{ASAR}\left(\mu\mathrm{mol/cm^2/min}\right) = \frac{N_d}{A\Delta t_{cycle}}, \tag{4}$$

where A is the projected area of the desalination cell and Δt_{cycle} is the cycle time. The use of two definitions of the ASAR help to evaluate and compare the design requirements of a desalination system by highlighting the influence of electrode mass and area used to achieve the removal rate. The volumetric energy consumption was determined as

$$\frac{1}{V_d}\int_{\Delta t_{cycle}} IV dt \tag{5}$$

where $IV > 0$. Productivity, P, defined as the volume of the diluate produced per unit time and projected face area of the desalination cell was calculated as

$$P = \frac{V_d}{A\Delta t_{cycle}}. \tag{6}$$

In this work, the P of the symmetric cell with NiHCF electrodes is twice as high as that for the MCDI cell with carbon electrodes at the same Q as the desalinated water is produced in the entire duration of the desalination cycle for NiHCF cell. Furthermore, the water recovery (WR), defined as the ratio of the volume of desalinated water produced during one cycle and the total volume of water treated in one cycle[41], was fixed at 50% for both the systems.

2.4. Theory

The theoretical understanding of the desalination performance of porous carbon electrodes in MCDI has been extensively reported in literature [47–49]. Recently, the theoretical framework has been extended to intercalation electrodes [44]. This theory is used in the current work to understand the desalination performance of present system. In short, we model the transport of ions in the spacers and the electrodes and the intercalation dynamics in the active particles. First, the transport of ions in the spacer channel is described by a mass balance including an advective term for the inflow in the y-direction:

$$\varepsilon_s\frac{\partial c}{\partial t} = \frac{\varepsilon_s}{\tau_s}D_i\left\{\frac{\partial^2 c}{\partial x^2} + z_i\frac{\partial}{\partial x}\left(C_i n\frac{\partial \phi}{\partial x}\right)\right\} - v_y\frac{\partial c}{\partial y}. \tag{7}$$

The ion flux in x-direction is described by the Nernst-Planck equation. The transport of ions in the pores of the electrodes is modeled in a similar manner:

$$\varepsilon_e\frac{\partial c}{\partial t} = \frac{\varepsilon_e}{\tau_e}D_i\left\{\frac{\partial^2 c}{\partial x^2} + z_i\frac{\partial}{\partial x}\left(c\frac{\partial \phi}{\partial x}\right)\right\} + aJ_{int}, \tag{8}$$

where aJ_{int} is the intercalation flux from the pores into the active particles normalized by the surface area of the active particles per unit volume of the electrode, a. Then the intercalation degree, ϑ, is governed by

$$c_{max}\varepsilon_v\frac{\partial \vartheta}{\partial t} = aJ_{int}, \tag{9}$$

where c_{max} is the maximum theoretical concentration of the cations in the active particles. Finally, we assume an equilibrium between the cations in the active particle and the electrolyte where the potential difference is given by the Frumkin isotherm

$$\phi_{ec} - \phi = \mu_c^{\dagger} - \ln\frac{\vartheta}{1-\vartheta} + \ln\frac{c^+}{c_{ref}} - g(\vartheta - 0.5), \tag{10}$$

where ϕ_{ec} is the dimensionless potential in the conductive carbon in the electrode and g is a cation-dependent constant, signifying the intercation repulsion in the active particles. The model predicts the effluent

Table 2
Input values for the parameters in the model used to predict the desalination behavior of a symmetric cell with NiHCF electrodes, adopted from [44].

Parameter	Value
Electrode thickness (μm)	200
Spacer thickness (μm)	500
Electrode porosity, ε_e	0.5
Spacer porosity, ε_s	0.7
NiHCF volume fraction in electrode, ε_v	0.55
Maximum cation concentration, c_{max} (M)	4.4
Interfacial area, A (cm^2)	20
Inter-ionic repulsion factor, g	4
Flowrate, Q (mL/min)	6.4 – 11.8
Diffusion coefficient in membrane, D_m (m/s)	5.5×10^{-9}
Initial intercalation degree, $\vartheta_{initial}$	0.5

concentration from both spacer channels and the evolution of the cell voltage, V, in time. The cell voltage is calculated as the difference between the ϕ_{ec} at the anode and the cathode of the desalination cell. The parameters used in the model are given in Table 2.

3. Results and discussion

3.1. Characterization of NiHCF powder and electrodes

The surface morphology of the NiHCF active particles after milling, observed under SEM, revealed a grainy structure of the active particles, as shown in Fig. S1 (a), that may have been formed due to inter-particle agglomeration. Imaging at different magnifications revealed particle sizes in the range of 0.5 to 5 μm. The porosity of these agglomerates affects the kinetics of ion transfer from the bulk to the active particles [44]. The SEM images revealed a combination of smooth and rough surfaces with micron-sized cracks. No evidence of active particle agglomeration and formation of island-like structures was observed.

An elemental analysis of the NiHCF active particles with ICP revealed the presence of Ni, Fe and Na in the ratio of 1.9:1.2:1. A deficiency in the amount of Na per formula unit, in comparison to the theoretical value can be attributed to the fast precipitation of NiHCF during synthesis [23]. This results in the formation of defective lattices with inclusion of water in them which can compete with sodium for insertion, as reported before [6,36]. The crystalline nature of the particles was confirmed by their X-ray diffractogram, which is comprised of sharp peaks at positions consistent with those of materials in the Fm3m space groups, as shown in Fig. S1 (b). In addition, the spectrum obtained was consistent with literature [45]. Finally, a N_2 adsorption analysis performed on the NiHCF powder revealed a BET surface area of $\approx$ 14 m^2/g, which is two orders of magnitude lower than the surface area of $\approx$ 2300 m^2/g, measured for the YP 80F carbon used in this study, which is also comparable to values reported in literature [46]. This shows that the mechanism of ion storage in the electrodes used is intercalation into the interstitial lattice sites of NiHCF electrodes.

3.2. Electrochemical characterization

The GIT technique, described in Section 2.2, was utilized to determine the total charge storage capacity of the NiHCF electrodes. The results of the electrochemical characterization of the NiHCF electrodes, as described in Section 3.2, are presented in Fig. S2. A negative current applied across the electrodes drives the Na^+ from the feed channel, through the macropores in the WE and into the interstitial sites of the NiHCF particles. Simultaneously, a Fe^{3+} in the lattice reduces to Fe^{2+} by transfer of an e^- from the current collector to the site of active particle *via* the conductive carbon. Such redox reactions accompanying ion intercalation are commonly observed for PBAs [36,50,51]. The equilibrium voltage (open circuit voltage (OCV)) of the NiHCF electrode (WE) relative to a Ag^+/AgCl electrode decreases as intercalation proceeds in time, making the electrode less favorable to the incoming Na ions. A reversal in the direction of the I results in the deintercalation of the adsorbed Na^+ and an increase in the OCV. During (de)intercalation, the NiHCF electrode acts as an anode/cathode, which makes it prone to pH-dependent faradaic reactions. These reactions degrade the electrode during deintercalation by oxidizing the nickel in the NiHCF into one of its oxides [38]. The pH of the electrolyte was kept around 3 to inhibit parasitic faradaic reactions. On average, a charge storage capacity of $\approx$ 55 mAh/g was recorded for the NiHCF electrode in this work, which is close to values reported in literature [6,30,45]. A lack of sodium in the synthesized PBA lattice, described in Section 3.1 is reflected in the capacity of the electrode obtained from the GITT, as it is lower than the theoretical charge storage capacity of $\approx$ 80 mAh/g, calculated for single cation intercalation per unit cell.

3.3. Desalination results

The first set of desalination tests, as mentioned in Section 2.3, were performed at three different c_{in} values: 20 mM (defined as the optimum CDI concentration [41]), 5 mM, and 50 mM for four I values: 2.5, 5, 10, and 15 A/m^2. The I changes direction when the cell voltage reaches a cutoff value of either -1 or 1 V. A sample data set, showing the concentration of the diluate, is given in Fig. 2 (a) & (b) for a feed of 20 mM treated in constant current mode at $I = 10$ A/m^2.

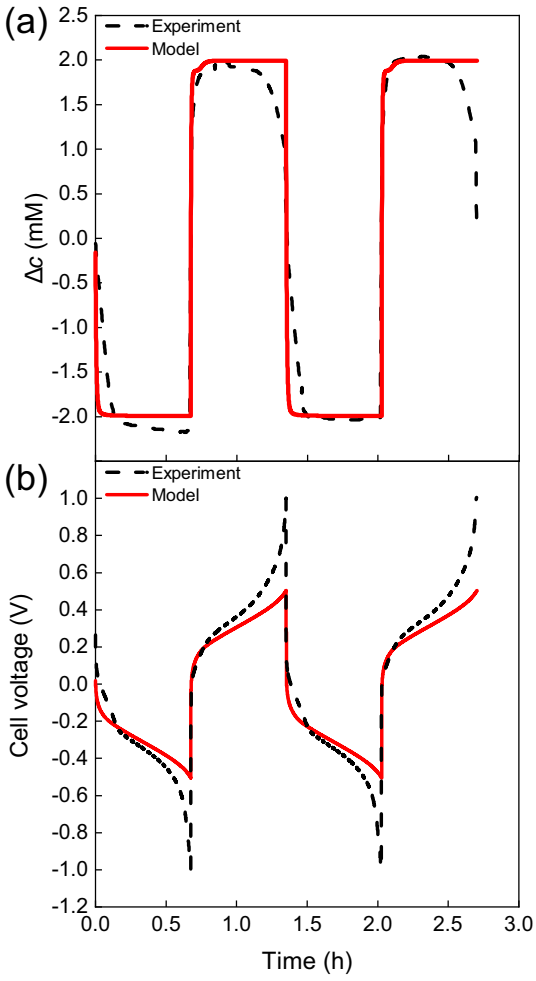

Fig. 2. Results of the desalination experiments (black dots) with superimposed model predictions (solid red line). The experimental data was obtained at the following conditions: $c_{in} = 20$ mM, $I = 10$ A/m^2 (a) Change in effluent concentration from one channel (Δc) with time for two desalination cycles (b) The cell voltage response between -1 and 1 V for two desalination cycles.

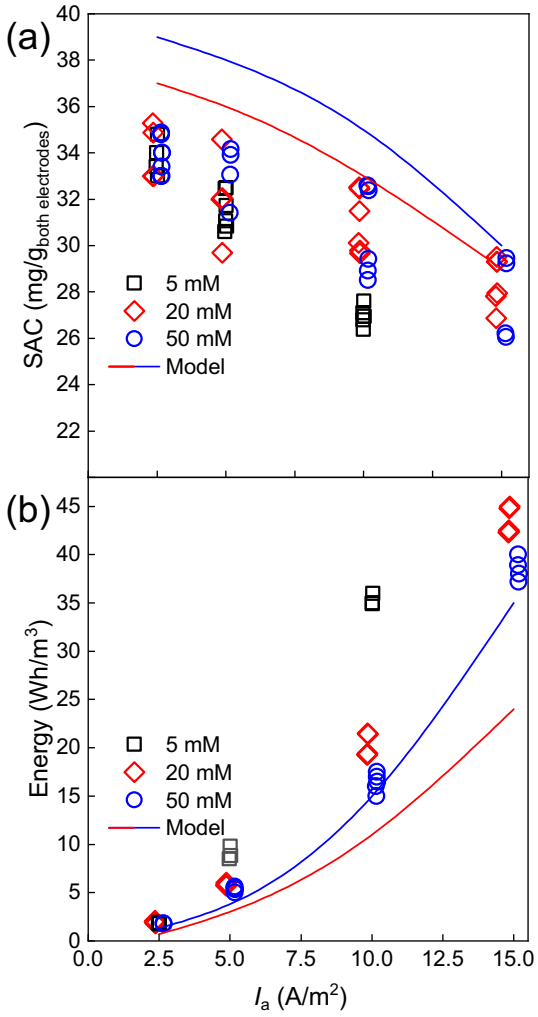

Fig. 3. Desalination results for symmetrical CDI cell with identical NiHCF electrodes. The experimental data is given for c_{in} = 5 (black squares), 20 (red diamonds), and 50 mM (blue circles). The corresponding model predictions for c_{in} = 20 and 50 mM are shown by solid red and blue lines **(a)** Single-channel SAC for different c_{in} as a function of I **(b)** Energy consumed in Wh/m^3 during (de)intercalation half cycles for different c_{in} as a function of I.

The salt concentration at the outlet from the cell changes in response to the I. This is confirmed in Fig. 2 (a) which gives Δc at the outlet for the diluate. At this I and Q, the $\langle \Delta c \rangle$ obtained was 2 mM, which increased and decreased with the I. Such dependence of Δc on I has been shown before for carbon electrodes in MCDI [52]. The Δc predictions from the ion transport model, with the parameter values mentioned in Table 2, are plotted as continuous red line. Clearly, these predictions were in agreement with the values obtained experimentally.

Fig. 2 (b) gives the corresponding change in the cell voltage during the constant current desalination at 10 A/m^2. The model prediction for the cell voltage are shown as a continuous red line. The voltage response of the cell was predicted in the model by an ion adsorption isotherm for monovalent ions given in Eq. (10). The trend in the cell voltage was qualitatively predicted and only lacked agreement with the experimental data at voltages approaching 1 and −1 V.

Fig. 3 (a) and (b) provide the SAC and the energy consumption data obtained for four different current densities: 2.5, 5, 10, and 15 A/m^2 at three different feed water concentrations: 5, 20, and 50 mM at a constant flowrate of 6.4 mL/min. The maximum SAC in one half cycle was measured at ≈ 35 mg/$g_{bothelectrodes}$ for the cell at the lowest I of 2.5 A/m^2. In one full desalination cycle, the total salt removed from the feed water was ≈ 70 mg/$g_{bothelectrodes}$. This highlights the advantage of a symmetric cell with two identical NiHCF electrodes that can continuously desalinate water without interrupting the process for regeneration. The SAC value for the intercalation half cycle decreased to 27 mg/$g_{bothelectrodes}$ when the I was increased to 15 A/m^2, as shown in Fig. 3 (a). At the same time, the $\langle \Delta c \rangle$ increased, as is shown in Fig. S3 (b). The decrease in SAC has also been observed for other intercalation materials during desalination [39], as the cut-off voltage is reached faster at higher I, resulting in a reduced half cycle time, as shown in Fig. S3 (a). During desalination, the concentration in the electrolyte-filled pores in the electrode may drop very low (< 1 mM) in the intercalation compartment [44]. So, at c_{in} = 5 mM, the highest I of 15 A/m^2 generates a high voltage drop in the cell, resulting in insignificant salt removal. Therefore, the salt removal for this condition was not included in Fig. 3. The model predictions, superimposed on the experimental data in Fig. 3, provide a qualitative estimate of the SAC obtained from the experiments. The overestimation in values can be attributed to the imperfect concentration prediction, as illustrated in Fig. 2 (a). The model estimates identical SAC values for I of 2.5 and 5 A/m^2. The SAC reduces at higher I, as obtained in the experiments as well. The theoretical results were omitted for the case of c_{in} = 5 mM and I = 15 A/m^2, as the model predicted a very high voltage drop over the cell and as a result, a low Δt_{HCT} and SAC.

Fig. 3 (b) represents the energy consumption for the desalination tests presented in Fig. 3 (a). The concentration increase reduces the ionic resistance in the cell and as a result, the energy consumption. In addition, a decrease in the half cycle times, Δt_{HCT}, with increasing I reduces the amount of treated water in one half cycle, increasing the volumetric energy consumption. The model predictions come close to the experimentally measured energy values for low I values, but lack a complete agreement at higher I. Therefore, a better understanding of an increase in the resistance of the system at high I and low c_{in} will be necessary in the future to accurately predict the energy consumption.

The results from the second set of experiments with symmetric NiHCF cell, for fixed Δt_{HCT}, are given in Figs. 4 (a) and (b). The dependence of the volumetric energy consumption on P is shown in panel (a) for two $\langle \Delta c \rangle$ values. The trend for each $\langle \Delta c \rangle$ shows an increase in the energy consumption with increasing P. Such dependence has also been reported before for carbon electrodes as well [41]. When the $\langle \Delta c \rangle$ was doubled from ≈ 1 to 2 mM, the energy consumption also doubled in the range of 50 ≤ P ≤ 125. To maintain a $\langle \Delta c \rangle$, I also increases with increasing P. The dependence of the energy consumption on I is plotted in Fig. S4. The predicted energy consumption by the model, given as a solid red line in Fig. 4 (a), matches with those obtained from the experiments. This follows from the agreement between the voltage curves obtained from the model and experiments, shown in Fig. 2 (b). Since the fixed Δt_{HCT} for the second set of experiments was only a fraction of the time it usually takes to saturate or empty the NiHCF electrodes, the model predictions closely match the energy values. This remains the case for all P at which the cell delivers $\langle \Delta c \rangle$ of ≈ 1 mM, and for a majority of P for $\langle \Delta c \rangle$ of ≈ 2 mM.

The performance of the CDI cell under constant voltage operation for a fixed Δt_{HCT} and P is given in Fig. 4 (b). The Q for these experiments was kept constant at 7.8 mL/min. The $\langle \Delta c \rangle$ increased with an increase in the applied voltage from 0.4 to 1.2 V. The maximum Δc, *i.e.* the difference between the lowest concentration recorded during adsorption and c_{in}, was ≈ 6 mM for the applied cell voltage of 1.2 V. This corresponds to a $\langle \Delta c \rangle$ of ≈ 5.5 mM for a fixed Δt_{HCT} of 3 mins. The energy consumption increased with the applied voltage in a similar manner as shown in Fig. 3 (b). Since the energy was normalized by the Δt_{HCT}, the actual duration of the half cycle had no influence on the energy consumption calculations. For the $\langle \Delta c \rangle$ of 5 mM, the NiHCF cell consumed ≈ 170 Wh/m^3 of energy at a P of 220 L/h/m^2. For comparison, data given in Fig. 5 of [41] shows that an MCDI cell with carbon electrodes consumes ≈ 140 Wh/m^3 (without recovery), and ≈ 60 Wh/m^3 (with recovery), to achieve a $\langle \Delta c \rangle$ of 5 mM at a P of 70 L/h/m^2, for a system with c_{in} = 20 mM and WR of 50%. Such comparisons

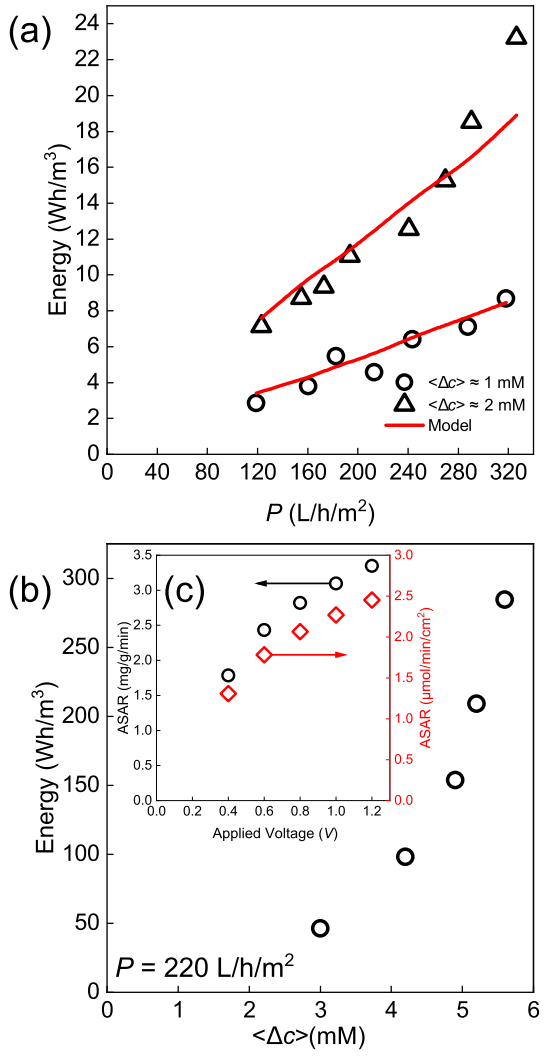

Fig. 4. Performance of the symmetric CDI cell with NiHCF electrodes during fixed Δt_{HCT} desalination tests in constant current and constant voltage modes (a) Variation of energy consumption of the cell under constant current operation as a function of P for $\langle\Delta c\rangle$ of ≈ 1 and 2 mM. The solid red line represents the predictions from the model for the identical operation conditions. (b) Energy consumption of the symmetric cell under constant voltage operation as a function of $\langle\Delta c\rangle$ at a fixed P of 220 L/h/m^2. The inset (c) gives the ASAR as a function of applied cell voltage in mg/g/min (left y-axis in black) and μmol/cm^2/min (right y-axis in red).

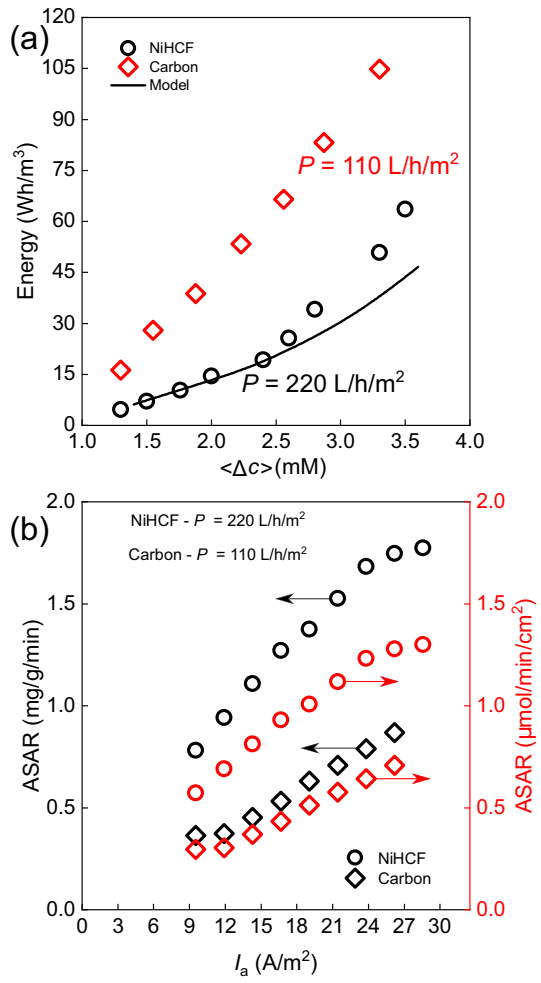

Fig. 5. Comparison of the symmetric CDI cell with NiHCF electrodes (circles) and MCDI cell with carbon electrode (diamonds) during fixed Δt_{HCT} desalination tests **(a)** Variation of energy consumption of the symmetric and MCDI cell under constant current operation with $\langle\Delta c\rangle$ for the same Q. The solid black line represents the predictions from the model for the symmetrical CDI cell with NiHCF electrodes **(b)** Variation of ASAR values in mg/g/min and μmol/min/cm^2 with the I for the symmetric and MCDI cell, obtained at the same Q.

are crucial to compare the performance of symmetric NiHCF cell with the data reported in CDI literature. In addition to the energy consumption, the rate of salt adsorption, ASAR, is also provided in Fig. 4 (c). The rate doubles from 1.6 mg/g/min, obtained at 0.4 V, to 3.2 mg/g/min, obtained at 1.2 V. The values of ASAR obtained here for the NiHCF cell are higher than the maximum ASAR of ≈ 1.8 and 2.5 mg/g/min, reported in literature for MCDI with carbon electrodes [53,54].

Finally, the results from the experiments performed to directly quantify the differences between NiHCF and carbon-based symmetric and MCDI cells is given in Fig. 5 (a) & (b). It must be pointed out that the Q was the same for the NiHCF and carbon cells. A sample data set containing the concentration and IV profiles from the NiHCF and carbon electrode cells, obtained during the fixed Δt_{HCT} comparison experiments, is given in Fig. S5. The desalination performance was evaluated on the basis of volumetric energy consumption as a function of $\langle\Delta c\rangle$, given in Fig. 5 (a), and the ASAR as a function of I, given in Fig. 5 (b). From panel (a), it can be concluded that for $\langle\Delta c\rangle \leq$ 2.5 mM and the same electrode weight, spacer thickness, and Δt_{HCT}, the MCDI cell with carbon electrodes consumed, on average, 3 times more energy than symmetric cell with NiHCF electrodes. As a specific example, the NiHCF cell consumes ≈ 22 Wh/m^3 at a P of 220 L/h/m^2 to deliver a $\langle\Delta c\rangle$ of 2.5 mM. The MCDI cell with carbon electrodes on the other hand consumes ≈ 65 Wh/m^3 to deliver the same $\langle\Delta c\rangle$ at a reduced P of 110 L/h/m^2. It must be pointed out that the symmetric NiHCF cell delivered twice as high P as the carbon-based MCDI cell at the same Q. For $\langle\Delta c\rangle >$ 2.5 mM, the MCDI cell still consumed > 2 times the energy consumed by the NiHCF cell. The relative increase in the energy consumption of the NiHCF cell, in comparison to the carbon-based MCDI cell, can be attributed to the transport limitations at higher adsorption or discharging rates, as has been reported before for other intercalation materials [39]. However, even at the highest I and $\langle\Delta c\rangle$ tested and achieved here, respectively, the MCDI cell with carbon electrodes consumed twice as much energy as the symmetric cell with NiHCF electrodes. The conclusion remains the same when the energy consumption is calculated in Wh/mol-NaCl, as shown in Fig. S6 of the ESI. This finding is in line with the conclusion of a thermodynamic comparison of energy consumption between intercalation and carbon electrodes, recently performed in [29]. Furthermore, this finding also serves as an experimental proof for claims made in [55] about intercalation based CDI cell being more energy efficient than a carbon based

MCDI cell. Charge efficiency, Λ, another important parameter defined as the ratio of charge adsorbed by the electrode to the external charge input to the electrode, provides an interesting insight in this comparison. For low I, therefore low Δc, the symmetric NiHCF cell exhibited a high Λ of 96%. However, with increasing I, the Λ reduced and settled at $\approx$ 75%. This was observed for the highest I of 30 A/m^2. An increased resistance in the cell at high I may be behind the drop in Λ. This explains the relative increase in the energy consumption of the symmetric NiHCF cell at high Δc over the MCDI cell, which exhibited a Λ of 92% at the lowest I and settled at a Λ of 86% for the highest I of 27.5 A/m^2. The Λ values of both the systems, for all I, is provided in Table S1 of the ESI. Furthermore, the model predictions for the NiHCF cell, given by solid black line in Fig. 5 (b) match with the values obtained from experiments, especially for the $\langle \Delta c \rangle \leq 2.5$ mM. At higher $\langle \Delta c \rangle$ values, the model underestimates the energy consumption, as has been observed earlier from the data in Figs. 3 and 4.

In addition to energy consumption, the ASAR values obtained with the NiHCF and carbon MCDI cells as a function of I are presented in Fig. 5 (b). The ASAR values, calculated for one full cycle of desalination for both cells, show that the NiHCF cell removed ions at a rate twice as high as that obtained for MCDI cell with carbon electrode. This further highlights the advantage of a two-chamber symmetric cell over a single-chamber MCDI cell: the NiHCF cell desalinated water in the entire cycle and delivered higher ASAR and P at the same Q. Comparison of ASAR values obtained during the constant current and constant voltage operation of the NiHCF cell shows that higher ASAR was achieved in the constant voltage mode in comparison to the constant current mode. This can be seen from Figs. 4 (b) and 5 (b). However, the energy consumption of the cell, plotted as a function of ASAR for constant current and voltage mode of operation in Fig. S7, was also found to be higher during the constant voltage operation. It is clear from the data in the figure that the constant voltage mode of operation renders higher rates of adsorption at the expense of the energy consumption.

4. Conclusion

In this study we demonstrated the intrinsically high energy efficiency of symmetric CDI cells with nickel hexacyanoferrate (NiHCF) electrodes compared to carbon-based MCDI cells by typically obtaining a 2.5-fold reduced energy consumption. In addition, the average salt adsorption rate (ASAR) of the NiHCF cell was typically 2-fold higher than that of a carbon-based MCDI cell for identical separation conditions. The set-up contained identical NiHCF electrodes which reversibly intercalate Na ions. This allowed for continuous desalination, and a removal of 70 mg NaCl/$g_{bothelectrodes}$ in one full cycle at an applied current of 2.5 A/m^2. An even higher ASAR was obtained in constant voltage mode in comparison to constant current mode, but at the expense of a higher energy consumption. A Nernst-Planck transport model, with Frumkin adsorption isotherm, was successfully used to accurately predict the SAC, *via* the effluent concentration. In addition, it provides a qualitative description of the energy input, *via* the cell voltage prediction, especially for the lower current densities tested here. A better theoretical understanding of the resistance in the NiHCF cell will be required to improve the energy input predictions also at higher current densities.

CRediT authorship contribution statement

Kaustub Singh: Conceptualization, Investigation, Formal analysis, Data curation, Writing - original draft. **Li Zhang**: Modelling, Writing - review & editing. **Han Zuilhof**: Writing - review & editing. **Louis C.P.M. de Smet**: Supervision, Data curation, Writing - review & editing.

Declaration of competing interest

All authors are aware of the submission and agree to its publication. The authors declare no conflict of interest.

Acknowledgement

This work was supported by the European Union Horizon 2020 research and innovation program (ERC Consolidator Grant to LdS, Agreement No. 682444) and was performed in the cooperation framework of Wetsus, European Centre of Excellence for Sustainable Water Technology. Wetsus is co-funded by the Dutch Ministry of Economic Affairs and Ministry of Infrastructure and Environment, the European Union Regional Development Fund, the Province of Fryslân, and the Northern Netherlands Provinces. The authors thank the participants of the research theme Capacitive Deionization for fruitful discussions and financial support, Dr. Maarten Biesheuvel for discussions on the theory, Dr. Slawomir Porada for discussions on the experiments, data presentation and writing, Dr. Rafael L. Zornitta for carbon characterization, Mr. Barend van Lagen for XRD analysis, Dr. Prashanth Kumar for SEM and EDS analysis, and Mr. Jelmer Dijkstra for Prussian blue BET measurements.

Appendix A. Supplementary data

Supplementary data to this article can be found online at https://doi.org/10.1016/j.desal.2020.114647.

References

[1] M.E. Suss, S. Porada, X. Sun, P.M. Biesheuvel, J. Yoon, V. Presser, Water desalination via capacitive deionization: what is it and what can we expect from it? Energy Environ. Sci. 8 (8) (2015) 2296–2319.
[2] P M Biesheuvel et al., Capacitive deionization–defining a class of desalination technologies, In: arXiv preprint arXiv:1709.05925 (2017).
[3] S. Porada, R. Zhao, A. van der Wal, V. Presser, P.M. Biesheuvel, Review on the science and technology of water desalination by capacitive deionization, Prog. Mater. Sci. 58 (8) (2013) 1388–1442.
[4] K.C. Smith, R. Dmello, Na-ion desalination (nid) enabled by na-blocking membranes and symmetric na-intercalation: porous-electrode modeling, J. Electrochem. Soc. 163 (3) (2016) A530–A539.
[5] J. Lee, K. Jo, J. Lee, S.P. Hong, S. Kim, J. Yoon, Rocking-chair capacitive deionization for continuous brackish water desalination, ACS Sustain. Chem. Eng. 6 (8) (2018) 10815–10822.
[6] S. Porada, A. Shrivastava, P. Bukowska, P.M. Biesheuvel, K.C. Smith, Nickel hexacyanoferrate electrodes for continuous cation intercalation desalination of brackish water, Electrochim. Acta 255 (2017) 369–378.
[7] J. Kang, T. Kim, H. Shin, J. Lee, J.I. Ha, J. Yoon, Direct energy recovery system for membrane capacitive deionization, Desalination 398 (2016) 144–150.
[8] P. Dlugolecki, A. van der Wal, Energy recovery in membrane capacitive deionization, Environmental Science & Technology 47 (9) (2013) 4904–4910.
[9] L. Wang, J. Dykstra, S. Lin, Energy efficiency of capacitive deionization, Environmental Science & Technology 53 (7) (2019) 3366–3378.
[10] Z.-H. Huang, Z. Yang, F. Kang, M. Inagaki, Carbon electrodes for capacitive deionization, J. Mater. Chem. A 5 (2) (2017) 470–496.
[11] S. Porada, M. Bryjak, A. van der Wal, P.M. Biesheuvel, Effect of electrode thickness variation on operation of capacitive deionization, Electrochim. Acta 75 (2012) 148–156.
[12] R.L. Zornitta, J.J. Lado, M.A. Anderson, L.A. Ruotolo, Effect of electrode properties and operational parameters on capacitive deionization using low-cost commercial carbons, Sep. Purif. Technol. 158 (2016) 39–52.
[13] R.L. Zornitta, F.J. Garca-Mateos, J.J. Lado, J. Rodrguez-Mirasol, T. Cordero, P. Hammer, L.A. Ruotolo, High-performance activated carbon from polyaniline for capacitive deionization, Carbon 123 (2017) 318–333.
[14] P. Ratajczak, M.E. Suss, F. Kaasik, F. Béguin, Carbon electrodes for capacitive technologies, Energy Storage Materials 16 (2019) 126–145.
[15] R. Zhao, O. Satpradit, H. Rijnaarts, P.M. Biesheuvel, A. Van der Wal, Optimization of salt adsorption rate in membrane capacitive deionization, Water Res. 47 (5) (2013) 1941–1952.
[16] P.M. Biesheuvel, R. Zhao, S. Porada, A. Van der Wal, Theory of membrane capacitive deionization including the effect of the electrode pore space, J. Colloid Interface Sci. 360 (1) (2011) 239–248.
[17] L. Han, K. Karthikeyan, M.A. Anderson, K.B. Gregory, Exploring the impact of pore size distribution on the performance of carbon electrodes for capacitive deionization, J. Colloid Interface Sci. 430 (2014) 93–99.
[18] Y. Li, C. Zhang, Y. Jiang, T.-J. Wang, H. Wang, Effects of the hydration ratio on the

electrosorption selectivity of ions during capacitive deionization, Desalination 399 (2016) 171–177.
[19] M.E. Suss, Size-based ion selectivity of micropore electric double layers in capacitive deionization electrodes, J. Electrochem. Soc. 164 (9) (2017) E270–E275.
[20] K. Singh, S. Porada, H.D. de Gier, P.M. Biesheuvel, L.C.P.M. de Smet, Timeline on the application of intercalation materials in capacitive deionization, Desalination 455 (2019) 115–134.
[21] M.E. Suss, V. Presser, Water desalination with energy storage electrode materials, Joule 2 (1) (2018) 25–35.
[22] A. Paolella, et al., A review on hexacyanoferrate-based materials for energy storage and smart windows: challenges and perspectives, J. Mater. Chem. A 5 (36) (2017) 18919–18932.
[23] J.-H. Lee, G. Ali, D.H. Kim, K.Y. Chung, Metal-organic framework cathodes based on a vanadium hexacyanoferrate prussian blue analogue for high-performance aqueous rechargeable batteries, Adv. Energy Mater. 7 (2) (2017) 1601491.
[24] H Kim, et al., $Na_2FeP_2O_7$ as a Promising Iron-Based Pyrophosphate Cathode for Sodium Rechargeable Batteries: A Combined Experimental and Theoretical Study, Advanced Functional Materials 29 (9) (2013) 1147–1155.
[25] K. Singh, Z. Qian, P.M. Biesheuvel, H. Zuilhof, S. Porada, L.C.P.M. de Smet, Nickel hexacyanoferrate electrodes for high mono/divalent ion-selectivity in capacitive deionization, Desalination 481 (2020) 114346.
[26] T. Kim, C.A. Gorski, B.E. Logan, Ammonium removal from domestic wastewater using selective battery electrodes, Environmental Science & Technology Letters 5 (9) (2018) 578–583.
[27] S. Kim, H. Yoon, D. Shin, J. Lee, J. Yoon, Electrochemical selective ion separation in capacitive deionization with sodium manganese oxide, J. Colloid Interface Sci. 506 (2017) 644–648.
[28] P. Srimuk, J. Lee, S. Fleischmann, M. Aslan, C. Kim, V. Presser, Potential-dependent, switchable ion selectivity in aqueous media using titanium disulfide, ChemSusChem 11 (13) (2018) 2091–2100.
[29] R. Wang, S. Lin, Thermodynamic reversible cycles of electrochemical desalination with intercalation materials in symmetric and asymmetric configurations, J. Colloid Interface Sci. 574 (2020) 152–161.
[30] J. Lee, S. Kim, J. Yoon, Rocking chair desalination battery based on prussian blue electrodes, ACS Omega 2 (4) (2017) 1653–1659.
[31] T. Kim, C.A. Gorski, B.E. Logan, Low energy desalination using battery electrode deionization, Environmental Science & Technology Letters 4 (10) (2017) 444–449.
[32] M. Pasta, C.D. Wessells, Y. Cui, F. La Mantia, A desalination battery, Nano Lett. 12 (2) (2012) 839–843.
[33] A.A. Karyakin, Prussian blue and its analogues: electrochemistry and analytical applications, Electroanalysis 13 (10) (2001) 813–819.
[34] A.L. Lipson, et al., Nickel hexacyanoferrate, a versatile intercalation host for divalent ions from nonaqueous electrolytes, J. Power Sources 325 (2016) 646–652.
[35] C.D. Wessells, S.V. Peddada, M.T. McDowell, R.A. Huggins, Y. Cui, The effect of insertion species on nanostructured open framework hexacyanoferrate battery electrodes, J. Electrochem. Soc. 159 (2) (2011) A98–A103.
[36] K. Hurlbutt, S. Wheeler, I. Capone, M. Pasta, Prussian blue analogs as battery materials, Joule 2 (10) (2018) 1950–1960.
[37] R.Y. Wang, B. Shyam, K.H. Stone, J.N. Weker, M. Pasta, H.-W. Lee, M.F. Toney, Y. Cui, Reversible multivalent (monovalent, divalent, trivalent) ion insertion in open framework materials, Adv. Energy Mater. 5 (12) (2015).
[38] P. Marzak, J. Yun, A. Dorsel, A. Kriele, R. Gilles, O. Schneider, A.S. Bandarenka, Electrodeposited Na − 2Ni[Fe(CN) − 6] thin-film cathodes exposed to simulated aqueous Na-ion battery conditions, J. Phys. Chem. C 122 (16) (2018) 8760–8768.
[39] S. Kim, J. Lee, C. Kim, J. Yoon, Na − $2FeP_2O_7$as a novel material for hybrid capacitive deionization, Electrochim. Acta 203 (2016) 265–271.
[40] B.W. Byles, B. Hayes-Oberst, E. Pomerantseva, Ion removal performance, structural/compositional dynamics, and electrochemical stability of layered manganese oxide electrodes in hybrid capacitive deionization, ACS Applied Materials & Interfaces 10 (38) (2018) 32313–32322.
[41] S.A. Hawks, A. Ramachandran, S. Porada, P.G. Campbell, M.E. Suss, P.M. Biesheuvel, J.G. Santiago, M. Stadermann, Performance metrics for the objective assessment of capacitive deionization systems, Water Res. 152 (2018) 126–137.
[42] M. Qin, A. Deshmukh, R. Epsztein, S.K. Patel, O.M. Owoseni, W.S. Walker, M. Elimelech, Comparison of energy consumption in desalination by capacitive deionization and reverse osmosis, Desalination 455 (2019) 100–114.
[43] S.K. Patel, M. Qin, W.S. Walker, M. Elimelech, Energy efficiency of electro-driven brackish water desalination: electrodialysis significantly outperforms membrane capacitive deionization, Environmental Science & Technology 54 (6) (2020) 3663–3677.
[44] K. Singh, H.J.M. Bouwmeester, L.C.P.M. de Smet, M. Bazant, P.M. Biesheuvel, Theory of water desalination with intercalation materials, Physical Review Applied 9 (6) (2018) 064036.
[45] C.D. Wessells, S.V. Peddada, R.A. Huggins, Y. Cui, Nickel hexacyanoferrate nanoparticle electrodes for aqueous sodium and potassium ion batteries, Nano Lett. 11 (12) (2011) 5421–5425.
[46] M. Aslan, M. Zeiger, N. Jäckel, I. Grobelsek, D. Weingarth, V. Presser, Improved capacitive deionization performance of mixed hydrophobic/hydrophilic activated carbon electrodes, J. Phys. Condens. Matter 28 (11) (2016) 114003.
[47] A. Hemmatifar, M. Stadermann, J.G. Santiago, Two-dimensional porous electrode model for capacitive deionization, J. Phys. Chem. C 119 (44) (2015) 24681–24694.
[48] S. Porada, L. Weinstein, R. Dash, A. van der Wal, M. Bryjak, Y. Gogotsi, P.M. Biesheuvel, Water desalination using capacitive deionization with microporous carbon electrodes, ACS Appl. Mater. Interfaces 4 (3) (2012) 1194–1199.
[49] P.M. Biesheuvel, H. Hamelers, M. Suss, Theory of water desalination by porous electrodes with immobile chemical charge, Colloids and Interface Science Communications 9 (2015) 1–5.
[50] J. Qian, C. Wu, Y. Cao, Z. Ma, Y. Huang, X. Ai, H. Yang, Prussian blue cathode materials for sodium-ion batteries and other ion batteries, Adv. Energy Mater. 8 (17) (2018) 1702619.
[51] B. Paulitsch, J. Yun, A.S. Bandarenka, Electrodeposited Na2VO x [Fe (CN) 6] films as a cathode material for aqueous na-ion batteries, ACS Appl. Mater. Interfaces 9 (9) (2017) 8107–8112.
[52] R. Zhao, P.M. Biesheuvel, A. Van der Wal, Energy consumption and constant current operation in membrane capacitive deionization, Energy Environ. Sci. 5 (11) (2012) 9520–9527.
[53] N. Kim, J. Lee, S.P. Hong, C. Lee, C. Kim, J. Yoon, Performance analysis of the multichannel membrane capacitive deionization with porous carbon electrode stacks, Desalination 479 (2020) 114315.
[54] R. Zhao, O. Satpradit, H.H.M. Rijnaarts, P.M. Biesheuvel, A. Van der Wal, Optimization of salt adsorption rate in membrane capacitive deionization, Water Res. 47 (5) (2013) 1941–1952.
[55] M. Metzger, M.M. Besli, S. Kuppan, S. Hellstrom, S. Kim, E. Sebti, C.V. Subban, J. Christensen, Techno-economic analysis of capacitive and intercalative water deionization, Energy Environ. Sci. 13 (2020) 1544–1560.